

TITLE OF SYMPOSIUM: 31st National Symposium on Fatigue and Fracture Mechanics

AUTHORS' NAMES:

Thomas J. Curtin and Robert A. Adey

TITLE OF PAPER:

Damage Repair Simulation of a Tension Panel and Pressurized Cylindrical Shell Using Adhesively Bonded Patches

AUTHORS' AFFILIATIONS:

Senior Applications Engineer, Computational Mechanics Inc. 25 Bridge Street, Billerica, MA 01821

Managing Director, Computational Mechanics BEASY, Ashurst Lodge, Southampton, SO40 7AA, UK

ABSTRACT: The bonded patch repair performance of a cracked tension panel, and a pressurized cylindrical shell with longitudinal through-crack, is simulated using a commercially available boundary element code. Three-dimensional, quadrilateral-shaped, reduced-quadratic order, boundary elements are used to model the panel, cylindrical shell, and repair patch. The adhesive layer is modeled using a continuously distributed system of linear springs. A special boundary element is used to model the crack. The tension panel analysis is based on a single-sided repair configuration. The relationship between crack length and stress intensity factor (SIF) for both the unrepaired and repaired panel is presented. The reduction in SIF and change in stress field, for the repaired panel compared to the unrepaired panel, determined from the present analysis, are compared with FEM and analytical results. The occurrence of out-of-plane bending and its impact on the through-thickness SIF variation in the panel is discussed. Crack growth simulation results show the crack front becoming curvilinear as the crack advances below the

patch. The reduction in SIF for a pressurized cylindrical shell with a double-sided elliptical patch repair is presented as a special case.

KEYWORDS: Bonded patch repair, three-dimensional boundary element analysis, stress intensity factor, crack propagation, pressurized cylindrical shell.

1.0 INTRODUCTION

Bonded repair techniques for damaged aircraft skin have become increasingly common given their advantage over more conventional repair methods that use mechanically fastened doublers; the major advantage being improved fatigue behavior. The ability to determine an acceptable fatigue life for the damaged structure has become increasingly important with the advent of the damage tolerance criteria mandated by FAA regulations for aging transport aircraft. In order to develop an effective bonded repair methodology it is important to be able to accurately determine the complex stress fields created by the repair as well as the resulting reduction in the stress intensity factor (SIF).

During the past decade extensive research has been conducted in the area of bonded patch repair performance. The majority of numerical analysis has been performed using the finite element method (FEM) [1, 2, 3, 4] although some work has also been done using the boundary element method (BEM) [5, 6, 7].

The present work focuses on the use of a three-dimensional boundary element analysis to investigate the bonded repair performance of both an edge-cracked and center-cracked tension panel, and a pressurized cylindrical shell with a longitudinal through-crack. The crack is modeled using the dual boundary element method (DBEM) [8, 9].

Previous BEM work has focused primarily on the use of two-dimensional elastostatic theory where the panel, patch, and adhesive have been assumed thin so that out-of-plane bending is not considered. Young [7] has performed patch repair studies using a BEM approach where both the patch and panel were discretized and the adhesive shear stresses were modeled as body forces acting on the patch and sheet. A straight crack in the sheet was modeled implicitly using a crack Green's function. Although this strategy avoids discretization of the crack surface it restricts the applications to straight cracks.

The present analysis extends the previous BEM work by performing a fully three-dimensional analysis and using the DBEM to model the crack. Although the DBEM method requires the crack surface to be discretized with special crack elements it also provides a means to analyze non planar cracks, investigate the out-of-plane behavior associated with single-sided patch repairs, and implement crack growth simulation studies. The present analysis also provides some preliminary results illustrating the use of the BEM to investigate the patch repair of an internally pressurized cylindrical shell.

Because the solution method and modeling technique of the BEM differ slightly from the FEM there are some inherent advantages and disadvantages in using the BEM for this type of analysis. Important advantages include simplified modeling of the adhesive layer, direct calculation of stress intensity factor (SIF) values, and accurate crack growth simulation. A disadvantage is that the BEM computer code used for this analysis is currently limited to geometrically linear analysis.

2.0 THREE-DIMENSIONAL BOUNDARY ELEMENT MODEL

The commercially available boundary element software, BEASY, is used to simulate the repaired behavior of a tension panel and pressurized cylindrical shell [10]. The plate and patch are modeled using a quadrilateral element topology and reduced-quadratic element order. The adhesive is modeled using a series of linear springs with stiffness values representing the adhesive material properties. The crack in the plate is simulated using a special boundary element capable of handling the discontinuous stress field located at the crack front. These important modeling features are discussed in detail in the following sections.

2.1 Simulation of adhesive layer

The adhesive is modeled as an interface boundary condition by applying internal springs on the surface shared between the patch and plate which are defined as different boundary element zones. The spring stiffness, specified in units of *pressure/displacement*, is defined in terms of the normal and tangential directions in a local coordinate system. The axial (k_{axial}) and shear (k_{shear}) spring stiffness are found from the following relationships:

$$\begin{aligned}k_{axial} &= \frac{E_a}{t_a} \\k_{shear} &= \frac{G_a}{t_a}\end{aligned}\tag{1}$$

The boundary element formulation for the internal spring relationship is defined by the following equation:

$$\mathbf{T}_{il} = k_i (\mathbf{u}_{i2} - \mathbf{u}_{il})\tag{2}$$

T_{il} = traction in the i^{th} direction acting on zone 1

k_i = spring stiffness in the i^{th} direction

u_{i1} = displacement of zone 1 in i^{th} direction

u_{i2} = displacement of zone 2 in i^{th} direction

The traction applied to zone 2 is the same in value as T_{i1} , but opposite in direction.

2.2 Simulation of Damage in the Plate

Cracks are modeled using the DBEM. The DBEM simultaneously imposes displacement and traction boundary integral equations on opposite sides of the crack surface. Both crack surfaces are discretized with discontinuous quadratic boundary elements. The SIFs are calculated from the crack opening displacements associated with node pairs on opposite crack surfaces using the near-tip displacement extrapolation method [8].

2.2.1 Discontinuous Elements

Discontinuous elements play an important role in the boundary element method because the problem variables are not forced to be continuous across elements. A discontinuous element is represented as an element where the mesh point and node locations are not coincident. As a result of this formulation the nodes are not shared between elements. The major benefit of discontinuous elements is their ability to model discontinuous stress results at a crack front.

2.2.2 Crack Propagation

Crack growth is simulated using an incremental type analysis. For the present analysis the incremental direction and size along the crack front for each extension are determined using the minimum strain energy density criterion. For each increment of crack extension, a stress analysis is performed using the DBEM, and the SIF are evaluated. The crack front is re-meshed and the next stress analysis is carried out for the new configuration. The theoretical aspects and

detailed mathematical formulation of this crack growth method are described in the work by Mi [11].

3.0 PROBLEM DESCRIPTION AND RESULTS

Computer modeling, using boundary element analysis, was performed to determine SIF solutions for a simple center-cracked plate and variety of patch repair configurations. Edge-cracked and center-cracked tension panels, repaired with composite and metallic patches respectively, are analyzed as well as the metallic patch repair of a cylindrical shell containing a longitudinal through-crack. The work is useful in demonstrating the accuracy and feasibility of the BEM as a repair simulation tool.

3.1 SIF Solution for Center-Cracked Tension Panel

A computer model of a 3 mm-thick tension panel, 500 x 500 mm in plan section, with a center-crack was created to determine the SIF for various crack lengths. The panel is loaded by a remote uniform tensile stress (1 MPa) applied normal to the crack. SIF solutions are determined for half-crack lengths ranging from 20 mm to 150 mm. In order to assess the accuracy of the boundary element solution the SIF values obtained from the present analysis are compared to analytical and FEM solutions for a similar configuration. The FEM solution used for comparison is presented in the work by Callinan [3]. This work discusses results from a three-dimensional, geometrically linear, finite element analysis. The center-cracked panel was modeled using 20-noded isoparametric brick elements. The SIF was determined using isoparametric wedge-shaped elements at the crack tip with the mid-point nodes shifted to the quarter-point locations to account for the crack tip singularity.

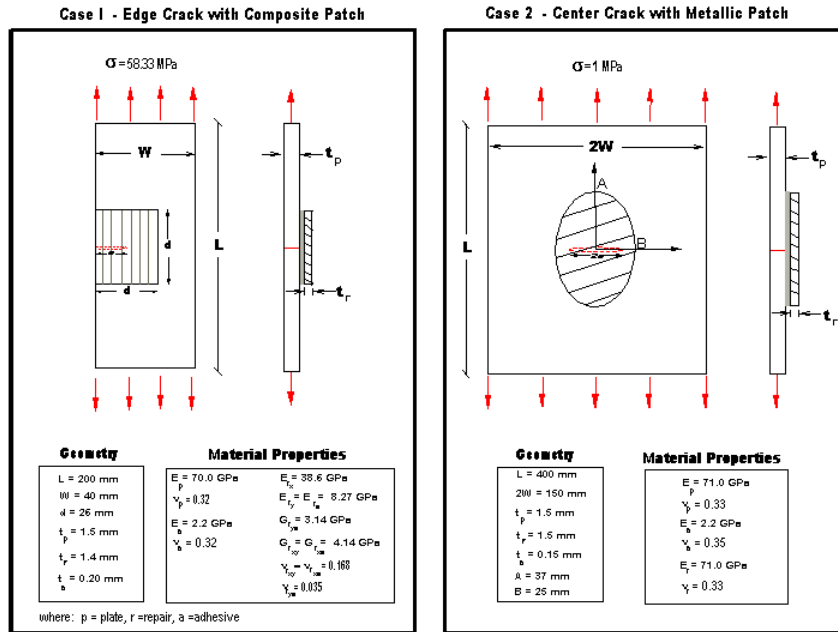


Figure 1. Composite and Metallic Patch Repair Configurations

Figure 1 shows a comparison of the SIF solutions obtained using the BEM, FEM, and analytical solutions. There is good agreement between the BEM, FEM, and analytical solutions for half-crack lengths less than 40 mm with the SIF values typically being within 1-3% of each other. For crack lengths between 40 and 120 mm the BEM solution agrees with the analytical solution almost exactly whereas the FEM solution ranges between 3-8 % higher than the analytical solution. At longer crack lengths, greater than about 120 mm, the analytical solution starts to diverge from the BEM solution. It should be noted that the analytical solution used to approximate the finite width boundary correction was determined by assuming a periodic array of collinear cracks in an infinite plate. Anderson [12] states that this analytical solution becomes less accurate for $a/W > 0.6$ (which in this case represents a half-crack length of 150 mm) and that numerical methods should be used to obtain a more accurate solution.

3.2 Bonded Patch Repair of Cracked Tension Panels

The following sections explore the feasibility of the BEM as an analysis/design tool for the bonded repair of thin sheet aluminum panels. Two different repair configurations are investigated and the results compared to either analytical or FEM solutions. Case 1 focuses on the modeling of an edge-cracked panel with a composite patch and Case 2 involves the analysis of a center-cracked panel with a metallic patch. The geometry, material properties, loading, and solution results for these two cases are presented in detail in the following sections.

3.2.1 Edge-Cracked Panel with Bonded Composite Patch (Case 1)

A computer model was created to determine the SIF for an edge-cracked panel with a single-sided, adhesively-bonded, composite repair. The patch was comprised of a glass-epoxy material with orthotropic elastic properties. The geometry and material properties are shown in Figure 2. A uniform load (58.33 MPa) was applied to the remote ends of the panel in a direction normal to the crack surface. This repair configuration and loading is the same as that investigated by Umamaheswar and Singh [2].

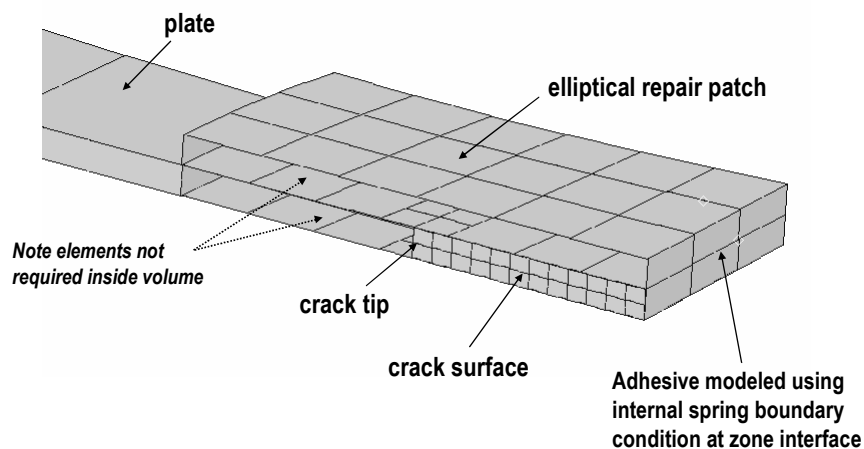


Figure 3. Boundary Element Mesh Showing Cut-Away View of Plate, Repair Patch and Crack Surface

Umamaheswar and Singh used finite element modeling to study the composite patch repair of an edge-cracked sheet. SIF solutions were obtained for the different combinations of brick, shell, and beam elements used to model the repair of the cracked sheet. The adhesive layer was modeled using both beam and brick elements. Brick elements were found to be more accurate and less labor intensive in terms of modeling time. Both geometrically linear and nonlinear FEM analyses were performed with results indicating that a geometrically nonlinear analysis provided a more accurate SIF solution. The SIF was determined by a modified crack closure integral method using the element nodal forces and displacements on the crack surface obtained from the FEM analysis.

A comparison of the SIF solutions, determined from the BEM and FEM analyses, is made in order to substantiate the accuracy of the boundary element solution and modeling approach. Table 1 shows the SIF result from the present analysis with comparison to the FEM result from the Umamaheswar and Singh study. The FEM case from [2], selected for comparison, used single brick elements to model the plate, adhesive, and patch. This FEM model was solved using a geometrically nonlinear analysis. In order to match the FEM result a convergence study was performed to determine the number of boundary elements required on the crack front for accurate SIF solution. The results (shown in Table 1) for BEM Model 4 indicate a favorable comparison with the FEM results, with the SIF value within approximately 1% of the FEM solution. However the comparison also raises the issue of the need for a geometrically nonlinear analysis. The following section attempts to quantify the error that results when using small displacement theory.

3.2.1.2 Solution Accuracy Using Small Displacement Theory

Typically the second order strain terms in the axial component of the strain field can be neglected for the configurations investigated in the present work if the out-of-plane bending effects are not significant. The complete axial component of the strain field for an isotropic plate can be simplified as shown in equation (3) since the second order axial $(\partial u_1/\partial x_1)^2$ and transverse $(\partial u_3/\partial x_1)^2$ strain terms are small in comparison to the axial strain $(\partial u_1/\partial x_1)$.

$$\varepsilon_{11} = \frac{\partial u_1}{\partial x_1} + \frac{1}{2} \left(\frac{\partial u_2}{\partial x_1} \right)^2 \quad (3)$$

The remaining second order term that needs to be investigated is the out-of-plane strain component $(\partial u_2/\partial x_1)^2$. The magnitude of this out-of-plane strain component was evaluated from displacement data obtained from the BEM analysis. The displacement data showed that an out-of-plane displacement of 0.091mm occurred over a half patch length of 13 mm. This translates into a second order strain effect of 24.5×10^{-6} mm/mm in accordance with equation (3). This value is small compared to the in-plane axial strain $(\partial u_1/\partial x_1)$ value of 833×10^{-6} mm/mm. The error introduced by neglecting this second order strain term is approximately 2.9% for this particular analysis.

3.2.2 Center-Cracked Panel with Bonded Metallic Patch (Case 2)

A second slightly different repair configuration was evaluated to help further understand the mechanics of the repaired configuration as well as the efficacy of the patch in reducing the SIF. This configuration is shown in Figure 2 and consists of a center-cracked panel repaired with a single-sided, adhesively-bonded, elliptical, metallic patch. A remote uniform tensile stress of 1 MPa was applied to the panel in a direction normal to the crack surface. A detailed

view of the boundary element mesh near the crack surface is shown in Figure 3. The computer model takes advantage of the symmetry plane passing through the middle of the crack. SIF results are obtained for half-crack lengths of 1.25, 5, 10, 17.5 and 22.5 mm. These results are compared to Rose's analytical solution for a similar case [13]. The shear stress and principal stress in both the patch and tension panel are presented to show the stress redistribution resulting from the repair. Results from a numerical crack propagation simulation are also presented to explore the nature of the crack front advancing below the repair.

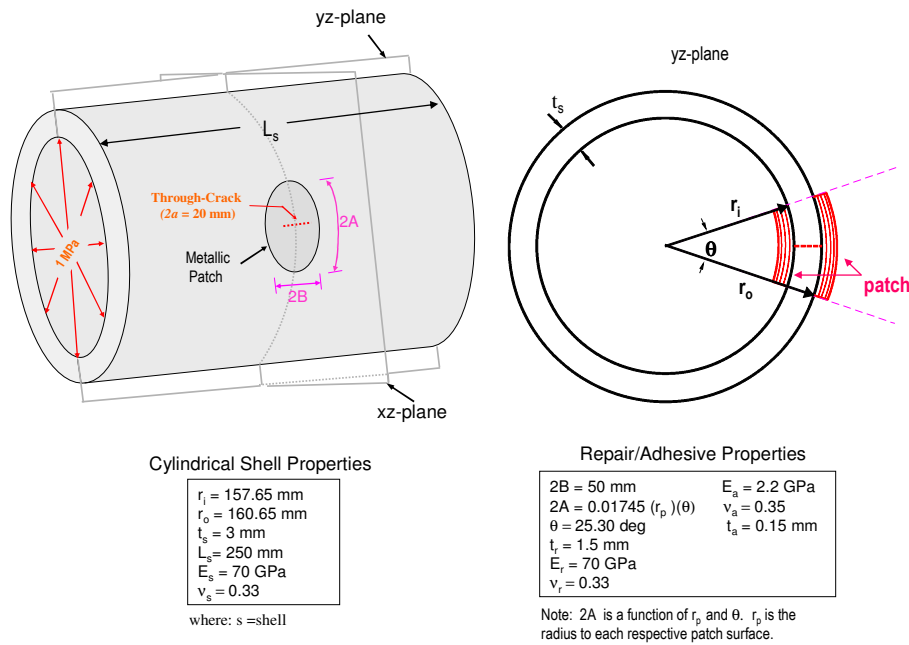


Figure 12. Metallic Patch Repair Configuration for Pressurized Cylindrical Shell

3.2.2.1 Stress Intensity Factor Solution

Rose derived an analytical solution for calculating the repaired stress-intensity factor (K_r) for a semi-infinite cracked plate with a bonded repair [13]. Rose's solution for a repaired stress-intensity factor is a function of both the joint flexibility and stress reduction under the patch.

Rose has proposed an upper bound for the repaired stress intensity factor (K_∞) which is

controlled primarily by the adhesive transfer length and applied stress. As such, K_{∞} , is very sensitive to the adhesive stiffness and the difference between the panel and repair patch stiffness.

For the single-sided repair configuration investigated, the difference in bending stiffness of the panel compared to the reinforced section results in a secondary bending moment. Rose provides an extension to his fundamental upper-bound analytical expression (K_{∞}) to account for this out-of-plane bending effect. The predicted SIF results and Rose's analytical solution for an upper bound limit with bending correction (\bar{K}_{∞}) are shown on Figure 4. These data indicate that the SIF solution approaches Rose's upper bound limit with increased crack length. The predicted SIF results shown on Figure 4 represent root-mean-square (K_{rms}) values computed using the membrane and bending components of the SIF (Table 2). The root-mean-square value of K calculated using equation (6), shown on Table 2, represents an average value that can be used for comparison with analytical estimates [3].

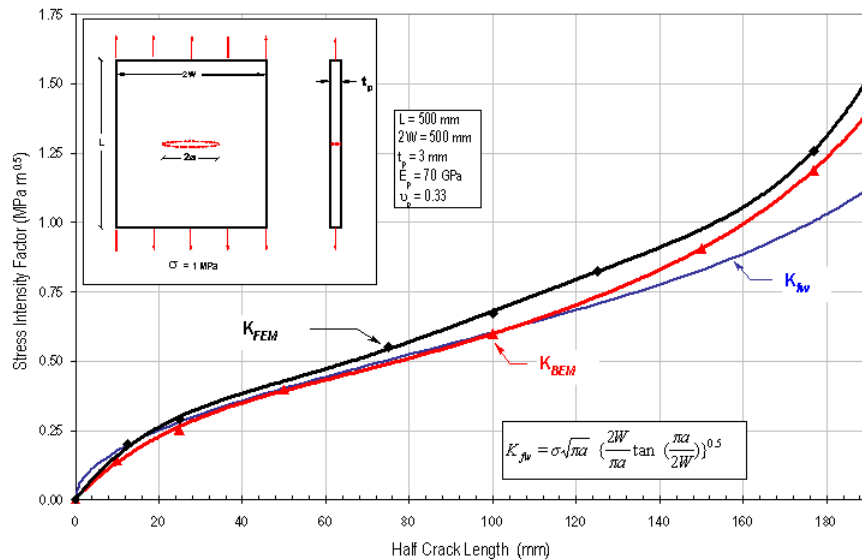


Figure 4. SIF Solution for Center-Cracked Plate

Figure 5 shows the deformed shape determined from the BEM analysis. The out-of-plane bending due to the one-sided reinforcement is well illustrated. The resulting shift in the neutral axis in the reinforced section creates a load path eccentricity and secondary bending moment in the repaired configuration.

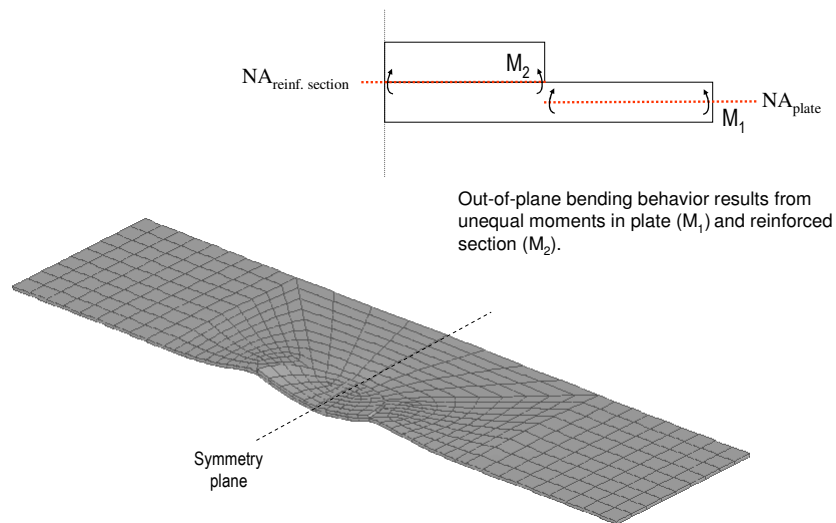


Figure 5. Deformed Shape of Center-Cracked Tension Panel with Single-Sided Elliptically-Shaped Metallic Patch

The through-thickness variation in the SIF for various crack lengths is shown on Figure 6. The plotted data represents SIF values computed automatically at crack element nodal points by the BEASY computer code. The data indicates a linear variation in the SIF with the difference in the value at the patch surface compared to the free surface increasing with increased crack length. These differences are 0.72, 1.21, and 2.33 MPa mm^{0.5} for half-crack lengths of 1.25, 5, and 17.5 mm respectively.

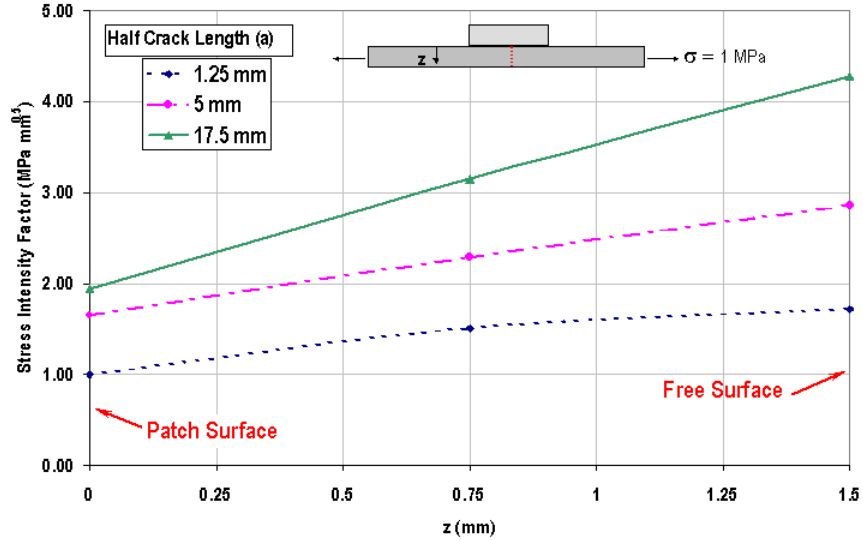


Figure 6. Through-Thickness SIF Variation for Single-Sided Metallic Patch Repair

3.2.2.2 Changes in Stress Field

Stress results for the repaired configuration with a half-crack length of 10 mm are used to illustrate the stress redistribution resulting from the repair. Figure 7 shows a contour plot of the shear stress and maximum principal stress on the repair patch. The highest maximum principal stress (1.45 MPa) occurs on the bottom surface of the repair patch, directly above the crack line [location A]. This stress represents an increase of approximately 30% above the far field stress. The contour plots of shear stress indicate two zones of high shear stress. The first zone [location B] occurs on the top surface of the patch opposite the crack tip and has a maximum shear stress of -0.16 MPa. The second zone occurs on the bottom edge of the patch [location C] and has a maximum shear stress of 0.15 MPa.

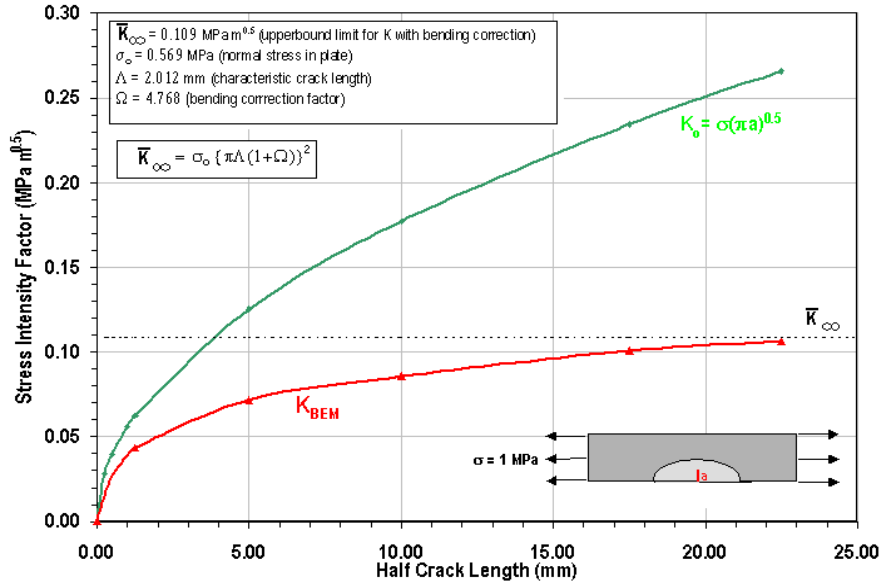


Figure 7. Plot Showing Reduced SIF for Single-Sided Metallic Patch Repair

Figure 8 shows the maximum principal stress distribution on the top and bottom surfaces of the tension panel near the patch boundary. The characteristic high stress at the crack tip [location D] is apparent on the bottom surface of the panel. With increased mesh refinement the crack tip stress should trend toward an infinite value since there is a stress singularity at this location. The principal stress distribution near the crack tip below the repair patch [location E] is characterized by a reduction in stress magnitude compared to the bottom surface of the panel. This is consistent with the load transfer from the cracked panel to the repair patch at this location.

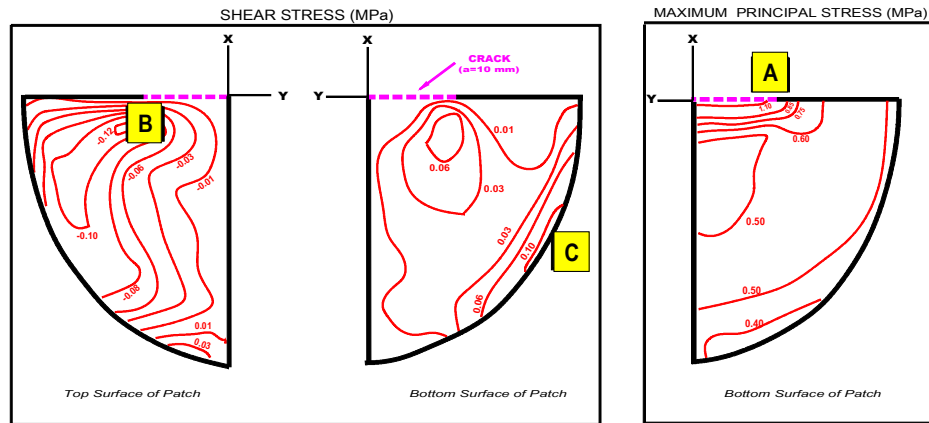


Figure 8. Contour Plots of Stress Field in Repair Patch.

A stress increase occurs on the bottom surface of the panel near the step change in thickness along the patch boundary [location F]. This stress increase is marked by the 1.40 MPa contour that follows the outline of the patch boundary. There is maximum compressive principal stress of -1.12 MPa and 5.61 MPa on the bottom and top surface of the panel respectively near the high curvature edge of the patch [locations G and H]. This high stress gradient through the thickness of the panel below the patch suggests very localized bending at the patch tip.

3.2.2.3 Numerical Crack Propagation Simulation

Figure 9 shows the crack growth path for a through-the-thickness crack of crack length $(2a) = 2.5$ mm, advanced in four crack step increments. The crack growth distances vary slightly for each step and are controlled by the maximum element size adjacent to the crack front. The maximum crack growth extension (Δa_{\max}) for each step is equal to the maximum element edge length on the crack front. Other points on the crack front are scaled relative to this maximum value. The crack growth increments displayed on Figure 9 are therefore a consequence of the maximum crack front element size and not a true indication of changes in crack growth rate between successive increments.

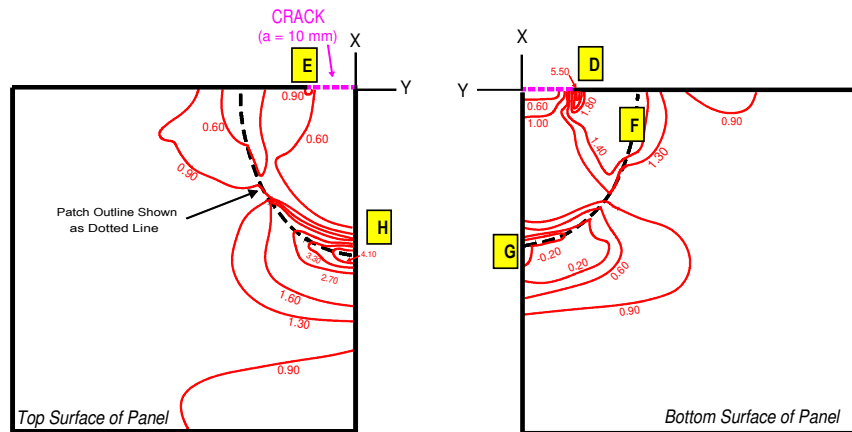


Figure 9. Contour Plot of Maximum Principal Stress in Tension Panel

The predicted crack fronts propagate in a nearly curvilinear fashion after the initial first step. This is consistent with the variation in the SIF along the crack front (Figure 10). The crack front grows fastest near the free end of the panel with each subsequent crack front being nearly parallel to the preceding crack front. With the exception of localized SIF values near the patch and free surfaces it appears that the SIF distribution along the crack front is approaching a nearly constant value. Increased refinement of the crack front mesh and additional crack step increments may provide a more accurate representation. It should be noted that the accuracy of the SIF values determined at the intersection of the crack front with the free surface should be viewed with some caution given that the stress singularity at this location varies from the typical $1/\sqrt{r}$ stress singularity.

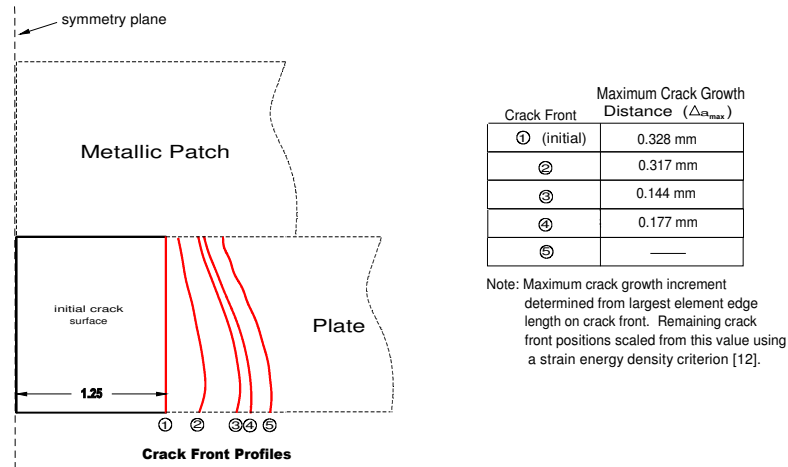


Figure 10. Predicted Crack Growth Path in Tension Panel with Single-Sided Repair

3.3 Bonded Patch Repair of Pressurized Cylindrical Shell

The boundary element solution and modeling approach used in the previous sections, to investigate repair of thin panels, is extended to investigate the fracture behavior of a cylindrical shell since this geometry is more representative of airframe structures. Computer models of both a cracked and repaired cylindrical shell are analyzed to determine the reduction in SIF. The numerical results provide data to help assess the influence of curvature on the SIF distribution and on the effectiveness of the bonded patch repair. The data presented in the following section is intended to characterize the variation in the SIF through-the-thickness of the shell for a single crack length.

3.3.1 Cylindrical Shell with Longitudinal Through-Crack

An internally pressurized cylindrical shell with a longitudinally oriented, 20 mm long, through-crack was analyzed to determine a SIF solution for this configuration. The nominal radius of the cylinder is 159.2 mm and the wall thickness is 3mm. The shell is modeled using material properties representative of a 7075 T6 aluminum alloy. The computer model assumes two planes of symmetry, the first through the midplane of the cylindrical shell at the crack location, and the second through the long axis of the cylindrical shell. A uniform internal

pressure of 1 MPa is applied to the inside face of the cylindrical shell. The SIF result is compared to the NASGRO solution for this configuration.

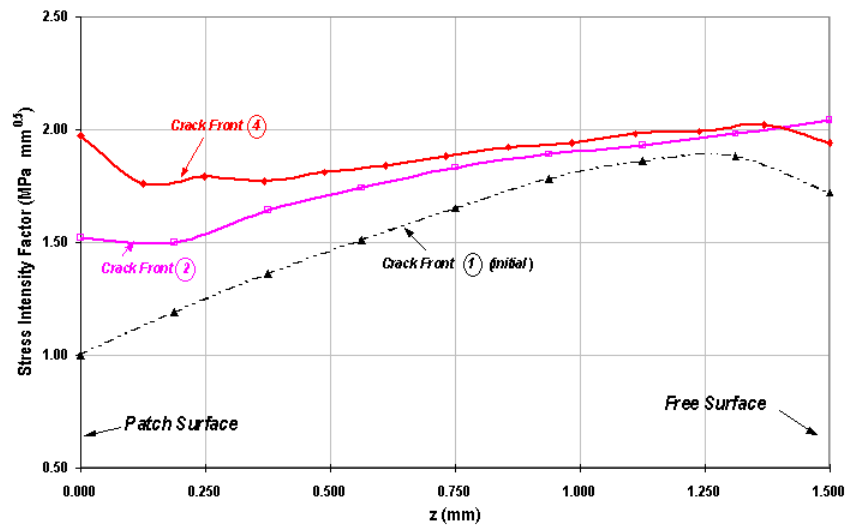


Figure 11. Change in SIF Distribution for Advancing Crack Front

Figure 11 shows the through-thickness SIF distribution for a pressurized cylindrical shell with longitudinal through-crack ($2a=20\text{mm}$). The data points shown in Figure 11 represent the SIF values along the crack front (located at 0.00, 0.75, 1.50, 2.25, and 3.00 mm from inner surface of the cylinder) determined from the boundary element analysis. A regression analysis (least squares fit) was performed and a second-order polynomial curve was fit to this data as a trendline. The data shown in Figure 11 indicates an approximately linear, through-thickness variation in the SIF solution. The SIF solution increases from the inside surface ($11.16 \text{ MPa m}^{0.5}$) to the outside surface ($12.71 \text{ MPa m}^{0.5}$) of the shell. Because the displacement in the circumferential direction controls Mode I crack opening, and the governing equations for a cylindrical shell define a linear increase in circumferential strain toward the outer shell surface, the SIF distribution obtained seems reasonable. The root-mean-square value ($11.76 \text{ MPa m}^{0.5}$),

computed from the data in Figure 11 is within 2.4% of the NASGRO solution ($11.48 \text{ MPa m}^{0.5}$) for this case [14].

This NASGRO solution was obtained by fitting a polynomial equation to three-dimensional, geometrically linear, FEM results for this configuration. The polynomial equation shown in the inset box on Figure 11 is based on a relationship between crack length ($2a$), wall thickness (t), and nominal cylinder radius (R). The NASGRO result represents an average through-thickness value. Further details on this formulation can be found in the work by Newman [15].

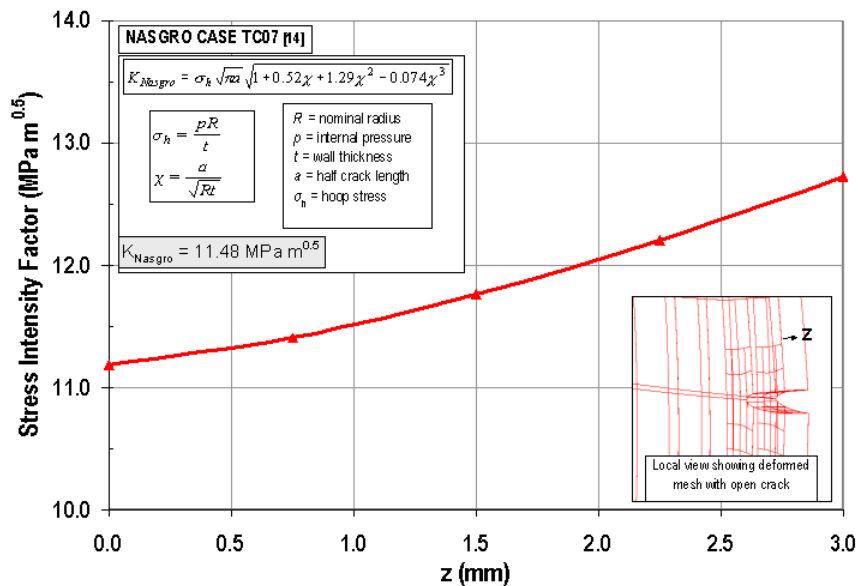


Figure 12. SIF Solution for Pressurized Cylindrical Shell with Longitudinal Through-Crack

3.3.2 Bonded Repair of Cylindrical Shell

The configuration described in the preceding section was modified to include a double-sided, elliptical, metallic patch. The repaired configuration and material properties are shown in Figure 12. The double-sided patch reduces the SIF value in the cracked cylindrical shell by a factor of approximately 6 (see Figure 13) and essentially eliminates the through-thickness

variation in the SIF. Because of the symmetric nature of the repair the use of a geometrically linear analysis for this case appears reasonable.

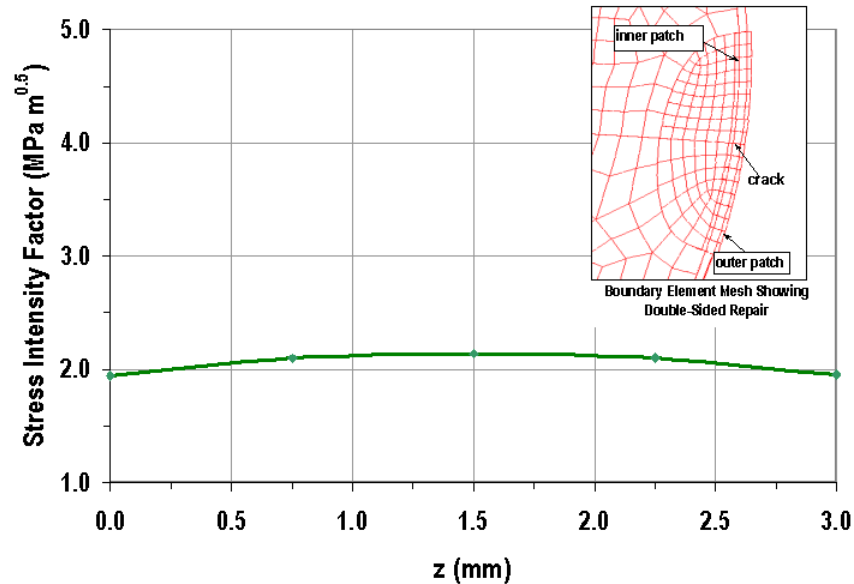


Figure 13. SIF Solution for Pressurized Cylindrical Shell with Double-Sided Metallic Repair Patch

4.0 CONCLUDING REMARKS

Computer modeling can be used to assess structural repairs made with bonded patches. The boundary element approach offers several advantages in this regard including:

- 1) Simplified modeling due to the surface only mesh requirement for the cracked structure and repair patch.
- 2) Efficient modeling of the adhesive using a zone interface boundary condition that eliminates the need for element discretization. Both the axial and shear properties of the adhesive can be modeled by simply creating a distributed system of springs with appropriate stiffness properties.
- 3) Direct computation of the SIF without the need to extract nodal forces or displacements for further postprocessing.

- 4) Crack propagation studies can be performed using the DBEM. The change in crack front morphology associated with growth below a bonded repair patch can be characterized.

The BEM modeling approach and solution methodology described in the present analysis provided good comparison with analytical and FEM solutions and should be explored further as means to conduct design assessment studies before implementing patch repairs.

5.0 REFERENCES

- [1] Kumar, A.M. and Singh, R., 1997, "3D Finite Element Modelling of a Composite Patch Repair", In: Proceedings of International Conference on Fracture, ICF-9, pp. 2159-2166.
- [2] Umamaaheswar, T.V.R.S., and Singh, R., 1998, "Modelling of a Patch Repair to a Thin Cracked Sheet", to be published in Engineering Fracture Mechanics, Elsevier Science Ltd.
- [3] Callinan, R.J., Rose, L.R.F., Wang, C. H., 1997, "Three Dimensional Stress Analysis of Crack Patching", In: Proceedings of International Conference on Fracture, ICE-9, pp. 2151-2158.
- [4] Sun, C.T., Lug, J., Arendt, C., 1996, "Analysis of Cracked Aluminum Plates Repaired with Bonded Composite Patches", AIAA Journal, Vol. 34, pp. 369-374.
- [5] Young, A., Cartwright, D.J., and Rooke, D.P., 1985, "Model Studies of Repair Patches", Proceedings of Int. Conf. on Fatigue, Corrosion, Cracking, Fracture Mechanics and Failure Analysis, Salt Lake City, pp. 339-346.
- [6] Salgado, N., 1998, Boundary Element Methods for Damage Tolerance Design of Aircraft Structures, Topics in Engineering Series, Vol. 33, Computational Mechanics Publications, Southampton UK and Boston USA.
- [7] Young A., Rooke, D.P., and Cartwright D.J., 1992, "Analysis of Patched and Stiffened Cracked Panels using the Boundary Element Method", Int. Journal of Solid Structures, Vol. 29, No.17, pp. 2201-2216.
- [8] Portela A. and Aliabadi, M.H., 1992, "The Dual Boundary Element Method: Effective Implementation for Crack Problems" International Journal for Numerical Methods, vol. 33, pp. 1269-1287.
- [9] Portela A., Aliabadi M.H., and Rooke D.P., 1993, "Dual Boundary Element Incremental Analysis of Crack Propagation", Computers & Structures, Vol. 46, No.2, pp. 237-247.

- [10] BEASY Reference Manual, Computational Mechanics Inc., Billerica, MA, 1999.
- [11] Mi, Y., 1996, Three-Dimensional Analysis of Crack Growth, Topics in Engineering Series, Vol. 28, Computational Mechanics Publications, Southampton UK and Boston USA.
- [12] Anderson, T.L., 1995, Fracture Mechanics, Fundamentals and Applications, CRC Press Inc. Boca Raton, Florida, 681 pp.
- [13] Rose, L.R.F., 1988, "Theoretical Analysis of Crack Patching", In: Bonded Repair of Aircraft Structures, edited by A. Baker and R. Jones, Martinus Nijhoff Publishers, pp. 77-106.
- [14] Fatigue Crack Growth Computer Program "NASGRO" Version 3.00, Reference Manual, Revision B, September 1998, NASA, 98 pp
- [15] Newman, J.C., Jr., "Fracture Analysis of Surface and Through Cracks in Cylindrical Pressure Vessels," NASA TN D-8325, December 1976.

TABLE 1 – Comparison of SIF Solutions for Case 1 - Edge Crack with Composite Patch

SIF Component (values in units of MPa \sqrt{m})	FEM Solution ⁽¹⁾	BEM Model 1	BEM Model 2	BEM Model 3	BEM Model 4
BEM Element Order ⁽²⁾	--	linear	linear	linear	reduced- quadratic
No. of Crack Front Elements	--	2	4	8	8
K_{patch} (patch surface) ⁽³⁾	4.73	3.89	3.68	3.78	4.70
K_{free} (free surface) ⁽³⁾	13.43	10.59	11.37	13.09	13.59
K_b (bending) ⁽⁴⁾	4.35	3.35	3.85	4.66	4.45
K_m (membrane) ⁽⁴⁾	9.08	7.24	7.53	8.44	9.15
K_{rms} (root mean square) ⁽⁵⁾	9.42	7.49	7.85	8.85	9.50
% K_{rms} deviation from FEM	--	20.5%	16.7%	6.1%	-0.7%

NOTES:

- 1) Represents reference solution for comparison with BEM results. FEM solution from work by Umamaheswar and Singh [2] using 8-noded, 24 DOF brick elements and geometrically nonlinear analysis.
- 2) Element order shown is for the tension panel and repair patch. Reduced-quadratic elements were used on the crack surface in all cases. Linear elements have 4 corner nodes. Reduced-quadratic elements have 4 corner nodes and 4 mid-side nodes.
- 3) K_{patch} and K_{free} represent the SIF values determined at the respective locations on the crack front directly by the BEASY computer code.
- 4) The bending (K_b) and membrane (K_m) SIF components are determined using the following relationships.

$$K_b = \left(\frac{K_{free} - K_{patch}}{2} \right) \quad (4)$$

$$K_m = \left(\frac{K_{patch} + K_{free}}{2} \right) \quad (5)$$

- 5) The K_{rms} value [3] is determined using the following equation and assumes a linear through-thickness variation in the SIF.

$$K_{rms} = \sqrt{K_m^2 + \frac{1}{3} K_b^2} \quad (6)$$

Table 2 – BEASY SIF Solutions for Repaired Tension Panel

a (mm)	K_{patch}	K_{free}	K_{b}	K_{m}	K_{rms}
1.25	0.032	0.054	0.011	0.043	0.044
5.00	0.052	0.090	0.019	0.071	0.072
10.00	0.058	0.111	0.026	0.084	0.086
17.50	0.062	0.135	0.037	0.099	0.101
22.50	0.064	0.144	0.040	0.104	0.106

NOTES:

(1) Units for SIF are $\text{MPa m}^{0.5}$